Vol. 33 (2002) ACTA PHYSICA POLONICA B No 5

PROSPECTS FOR THE DETERMINATION OF THE CHARGED HIGGS MASS AND $\tan\beta$ WITH THE ATLAS DETECTOR AT THE LARGE HADRON COLLIDER

Kétévi Adiklè Assamagan

Brookhaven National Laboratory, Upton, NY 11973 USA

and Yann Coadou

Uppsala University, Uppsala, Sweden

(Received January 23, 2002)

The observation of one or several Higgs bosons will be fundamental for the understanding of the electroweak symmetry breaking mechanism. In the Standard Model (SM), one scalar doublet is responsible for the electroweak symmetry breaking, leading to the prediction of a single Higgs boson. The simplest extension to the SM Higgs sector is the two Higgs doublet model present in many extensions to the SM itself, including supersymmetry. In such models, symmetry breaking leads to five Higgs particles, three neutral and a charged pair. The sensitivity of the ATLAS detector to the discovery of the charged Higgs has been studied in detail. In this paper, we discuss the expected precisions on the charged Higgs mass and $\tan\beta$ measurements at the Large Hadron Collider (LHC).

PACS numbers: 12.60.Jv, 14.80.Cp

1. Introduction

The Higgs sector of the Minimal Supersymmetric Standard Model (MSSM) contains five physical states, two of which are charged, $H^{\pm}$, and the other three are neutral (h^0, H^0, and A^0) [1]. The sensitivity of the ATLAS detector to the discovery of the charged Higgs has been investigated in detail [2]. Some of these studies have been carried out as particle-level event generation in PYTHIA [3] at $\sqrt{s} = 14$ TeV, with the detector resolutions and efficiencies parameterized in ATLFAST [4] from the full detector simulations. It has been assumed that the mass scale of supersymmetric partners of ordinary matter is above the charged Higgs mass so that charged Higgs decays into supersymmetric partners are forbidden. A central value of 175 GeV is used for the top-quark mass.

Below the top-quark mass, the charged Higgs is produced in top decays, $t \to bH^{\pm}$. In this mass range, the decay channel $H^{\pm} \to \tau\nu$ has been studied extensively for ATLAS and the signal appears as an excess of τ leptons [5]. The channel $H^{\pm} \to Wh^0$ is only relevant in a tiny range of MSSM parameter space although it constitutes a unique test for MSSM and may be sensitive to the singlet extension to MSSM, *i.e.*, NMSSM [6, 7]. The prospects for the determination of the charged Higgs mass and $\tan\beta$ below the top-quark mass has not yet been investigated.

In the transition region, *i.e.*, for $m_{H^{\pm}}$ just below or around the top-quark mass, the relevant channels are $H^{\pm} \to t^{*}b$ and $H^{\pm} \to \tau\nu$. However, for the correct description of the charged Higgs production and decay mechanisms in this region of parameter space, it is mandatory to use the production process $gg \to tbH^{\pm}$ which includes $gg \to t\bar{t}$ with $t \to bH^{\pm}$, the Higgs-strahlung mechanism and the relative interferences [8]. The 5-σ discovery contour of figure 1 shows a gap in the m_A axis around $m_A = 160$ GeV because charged Higgs studies have not yet been carried out for this region.

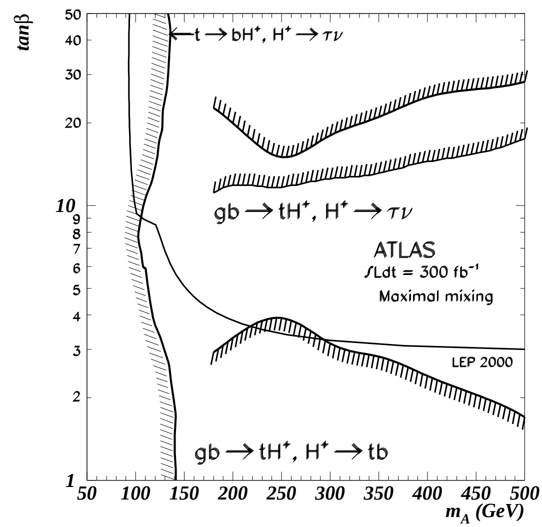

Fig. 1. The ATLAS 5-σ discovery contour of the charged Higgs. Below the top-quark mass, the charged Higgs is produced from top decay and the $\tau\nu$ channel provides coverage for most $\tan\beta$. Above the top-quark mass, the tb channel covers the low and the high $\tan\beta$ regions while the $\tau\nu$ channel extends the discovery reach to high Higgs masses and to lower $\tan\beta$ in the high $\tan\beta$ region.

Above the top-quark mass, the $2 \to 2$ production process $gb \to tH^{\pm}$ has been used and the decay channels $H^{\pm} \to tb$ and $H^{\pm} \to \tau\nu$ studied in detail [9, 10]. In the $H^{\pm} \to tb$ channel, upwards of 5-σ discovery can be achieved above the top-quark mass in the low and high $\tan\beta$ regions up to $\sim$ 400 GeV [9]. $H^\pm \to \tau\nu$ extends the discovery reach to high Higgs masses and to lower $\tan\beta$ values in the high $\tan\beta$ region as seen in figure 1. However, in the low $\tan\beta$ region, the $\tau\nu$ channel offers no sensitivity for the charged Higgs discovery as the $H^\pm \to \tau\nu$ branching vanishes [10]. In this paper, we discuss the expected precisions on the charged Higgs mass and $\tan\beta$ measurements with the ATLAS detector — above the top-quark mass — in the $H^\pm \to tb$ and $H^\pm \to \tau\nu$ channels.

2. $H^\pm$ mass determination in $H^\pm \to \tau\nu$

This channel does not offer the possibility for the observation of a resonance peak above the background, only the transverse Higgs mass can be reconstructed because of the presence of the neutrino in the final state. The background comes from single top, Wt, and $t\bar{t}$ productions with one $W \to \tau\nu$. Thus, the transverse mass is kinematically constrained to be less than the W-boson mass while in the signal, the upper bound is the charged Higgs mass. Furthermore, because the charged Higgs is scalar and the W-boson a vector, the polarization of the decay τ in the signal is different from the background case, particularly in the one-prong hadronic τ decays [11].

The differences in the event topology and in the τ polarization have been used to suppress the backgrounds in the studies reported in [10, 12], so that above the W mass threshold, the background in this channel is relatively small as shown in figure 2. As a result, although there is no reconstruction

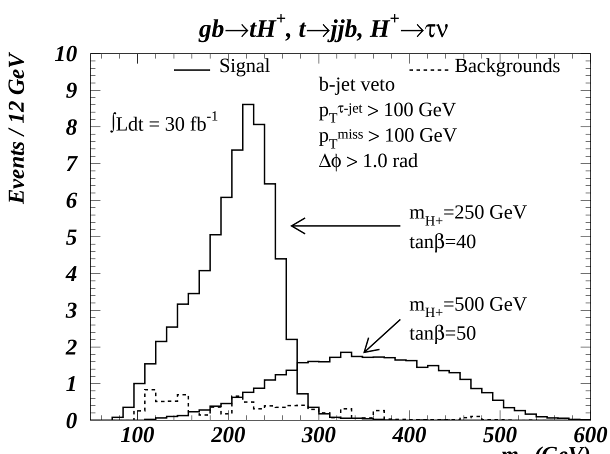

Fig. 2. The reconstruction of the transverse Higgs mass in $H^\pm \to \tau\nu$ for 250 and 500 GeV. The background is relatively small in this channel. The discovery reach is limited to high $\tan\beta$ but extended to higher masses compared to the tb channel.

of the resonance peak in this channel, the Higgs mass can be extracted from the transverse mass distribution with a relatively good precision. For the mass determination in this channel, we use the likelihood method presented in [13] and summarized in the following section.

2.1. Statistical uncertainties

Suppose we wish to estimate the expected precision and uncertainty on a Higgs reference mass m_0. We generate samples of events with charged Higgs masses, $m_k = m_0 + k \times \Delta m$ and for each m_k we perform dedicated selections presented in [10] in order to obtain the final signal+background mass distributions. For example, for a charged Higgs reference mass $m_0 =$ 250 GeV, one might generate signal events at Higgs masses $m_k =$ 230, 235, 240, 245, 250, 255, 260, 265 and 270 GeV. Subsequently, the reconstructed transverse mass distributions are smoothed, normalized to unity and fitted to obtain the associated probability density functions $\mathcal{P}_k(m)$.

The reference masses considered in this analysis and their corresponding probability density functions (signal+backgrounds) obtained from the transverse mass distributions are shown in figure 3. One can see a clear dependence on the charged Higgs mass: both edges (especially the leading edge) are shifted towards higher transverse masses as the input mass increases. The background is small enough not to spoil the sensitivity.

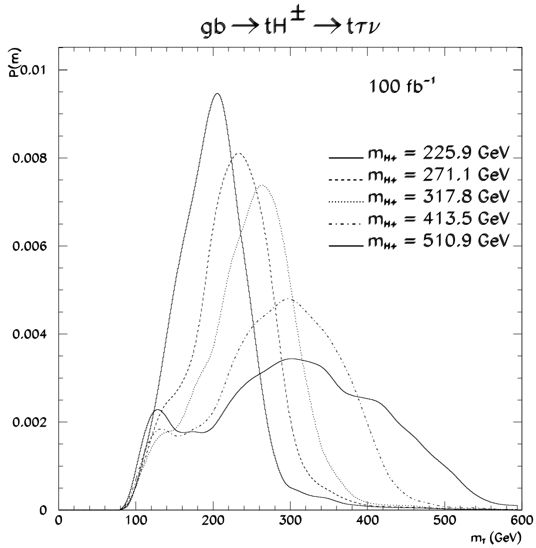

Fig. 3. The probability density functions (signal + background) obtained from distributions of the reconstructed transverse masses for the reference masses considered.

From the probability density function $\mathcal{P}_0(m)$ of the reference mass, a set $\{m_j\}_{j=1..N}$ of transverse masses is drawn, where $N = N_0 + \delta N_0$ and N_0 is the expected number of signal and background events for the reference mass m_0 with a Gaussian fluctuation δN_0. For each mass m_k the Likelihood function is computed:

$$\ln \mathcal{L}_k = \sum_{j=1}^{N} \ln \mathcal{P}_k(m_j)\,. \tag{1}$$

In figure 4, we show the difference $\Delta(\ln \mathcal{L}_k) = \ln \mathcal{L}_0 - \ln \mathcal{L}_k$ as function of m_k for one reference mass m_0. Around the minimum, which should be at m_0, we do a parabolic fit to get the actual expected charged Higgs mass. This exercise can be repeated many times within the statistical error δN_0 and the distribution of the expected values, so obtained, of the mass would be a Gaussian whose mean is the reconstructed mass and whose standard deviation is the statistical precision of the reconstructed mass as shown in figure 5.

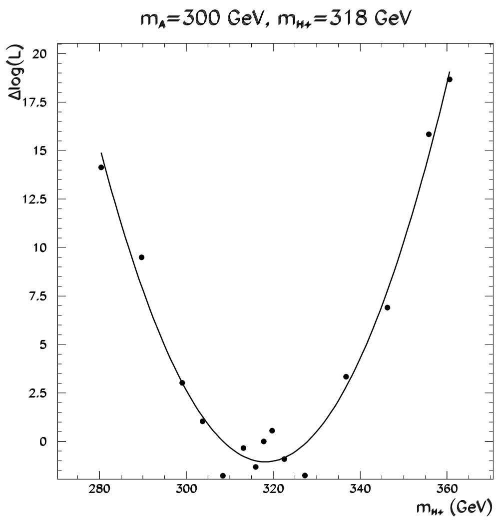

Fig. 4. The differences in the likelihood functions, $\Delta(\ln \mathcal{L}_k)$, versus the corresponding mass m_k. A parabolic fit is performed around the minimum and the minimum of the parabola is taken as the reconstructed mass. This Monte Carlo experiment can be repeated several times within the statistical uncertainty to get a distribution of the reconstructed mass.

Table I shows the expected statistical errors on the reference masses considered. At higher Higgs masses, the precisions worsen as the signal rate decreases. The slight offset between the reconstructed value and the reference mass is due to uncertainties in the probability density functions. The precision improves at higher luminosity, as expected.

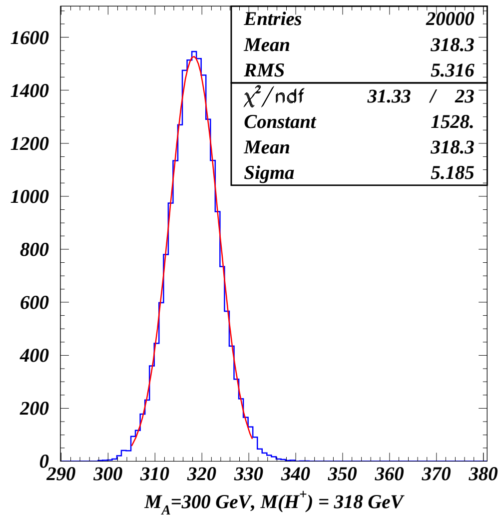

Fig. 5. The distribution of the mass obtained from the parabolic fit is a Gaussian whose mean is taken as the expected reconstructed mass and the standard deviation of the Gaussian is the precision of the mass. In this particular case, the reference mass is $m_0 = 317.8$ GeV. The reconstructed mass obtained from the likelihood analysis is 318.3 GeV with a statistical precision δm of 5.2 GeV. The deviation of the reconstructed value from the actual reference mass is due to uncertainties in the probability density functions.

TABLE I

The statistical precision of the mass determination in the $H^\pm \to \tau\nu$ channel. The reference masses are listed in the first column. The reconstructed masses $\langle m\rangle$ (GeV) and the corresponding precision δm (GeV) are calculated for 100 and 300 fb^{-1}. We take $\tan\beta = 45$. The statistical precision deteriorates as the Higgs mass increases because of the reduction in rate.

$m_{H^\pm}$ (GeV)	$\mathcal{L} = 100$ fb^{-1}		$\mathcal{L} = 300$ fb^{-1}	
m_0	$< m >$	δm	$< m >$	δm
225.9	226.4	3.0	226.4	1.7
271.1	271.0	3.4	271.1	2.0
317.8	318.3	5.2	318.3	3.0
365.4	365.5	7.8	365.7	4.6
413.5	413.6	7.7	413.8	4.5
462.1	462.3	10.2	462.6	6.0
510.9	511.5	13.0	511.9	7.4

2.2. Systematic uncertainties

Three main sources of systematic uncertainties are included in the mass determination: the shape of the background, the background rate and the energy scale. The background shape becomes more significant at lower Higgs masses, where there is more overlap between signal and background. To include this effect, we assumed a linear variation of the background shape, from -10% to $+10\%$ between the minimum and the maximum of the transverse mass distribution. Another source of systematic uncertainty is the rate of the backgrounds. It is expected that the background rate (Wt and $t\bar{t}$) could be known to 5% [13]. Therefore, to take this effect into account, we increase the background rate by 5% while at the same time we decrease the signal by 5%. Finally, we also include the scale uncertainty: 1% for jets and 0.1% for photons, electrons and muons. In Table II, we show the effects of the systematic uncertainties: the overall uncertainty in the mass determination is dominated by statistics.

TABLE II

The systematic effects on the mass determination in the $H^\pm \to \tau\nu$ channel are small. Columns 2 and 3 show the statistical uncertainties for an integrated luminosity of 300 fb^{-1}. Columns 4 and 5 include the systematic uncertainties. The total uncertainties are dominated by the statistical errors.

$m_{H^\pm}$ (GeV)	No systematics		With systematics	
	$< m >$	δm	$< m >$	δm
225.9	226.4	1.7	225.9	1.7
271.1	271.1	2.0	270.9	2.3
317.8	318.3	3.0	319.9	3.5
365.4	365.7	4.6	365.2	4.7
413.5	413.8	4.5	414.9	4.7
462.1	462.6	6.0	460.8	6.3
510.9	511.9	7.4	511.7	9.2

3. $H^\pm$ mass determination in $H^\pm \to tb$

In the tb channel, the full invariant mass can be reconstructed as shown in figure 6 although this channel suffers from the large irreducible $t\bar{t}b$ background and also from the signal combinatorial background. The determination of the mass can be done using the likelihood method described above or by fitting the signal and the background. In the latter case, one assumes that the background shape and normalization can be determined by fitting outside the signal region, thus, the systematic uncertainties include only the scale uncertainty. We assume a Gaussian shape for the signal and an exponential for the background and fit signal+background including the statistical fluctuations and the scale uncertainty.

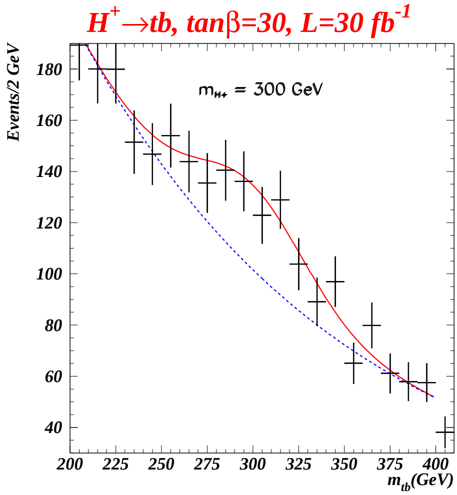

Fig. 6. The reconstructed tb invariant mass in the $H^\pm \to tb$ channel shows a resonance peak although this channel suffers from large $t\bar{t}b$ and signal combinatorial backgrounds. The likelihood method can be used to estimate the expected precision of the mass determination. It is also possible to fit the signal and background directly assuming the background shape and normalization can be constrained by fitting outside the signal region. Both methods are in agreement on the mass determination.

The probability density functions used for the mass determination in $H^\pm \to tb$ by the likelihood method are shown in figure 7. One can conclude that the presence of the background decreases the sensitivity to the signal, whereas in the $H^\pm \to \tau\nu$ channel, the background has a marginal impact on the sensitivity. Nevertheless, as shown in Table III, the precisions on the mass determination from the likelihood and fitting methods are comparable.

TABLE III

In the $H^\pm \to tb$ channel two different methods are used for the mass determination: the likelihood method and the fit to signal and background. The results from both methods are in agreement. At the lowest Higgs mass point the fitting method does not work because signal and background shapes are very similar. The results are shown for an integrated luminosity of 100 fb^{-1}.

$m_{H^\pm}$ (GeV)	Likelihood		Fit	
	$\langle m\rangle$	δm	$\langle m\rangle$	δm
225.9	226.9	1.8		
271.1	270.1	10.1	271.0	10.3
317.8	320.2	11.3	316.4	11.5
365.4	365.4	12.1	363.8	12.5
413.5	417.4	17.6	412.6	17.9
462.1	465.9	24.1	460.4	24.4

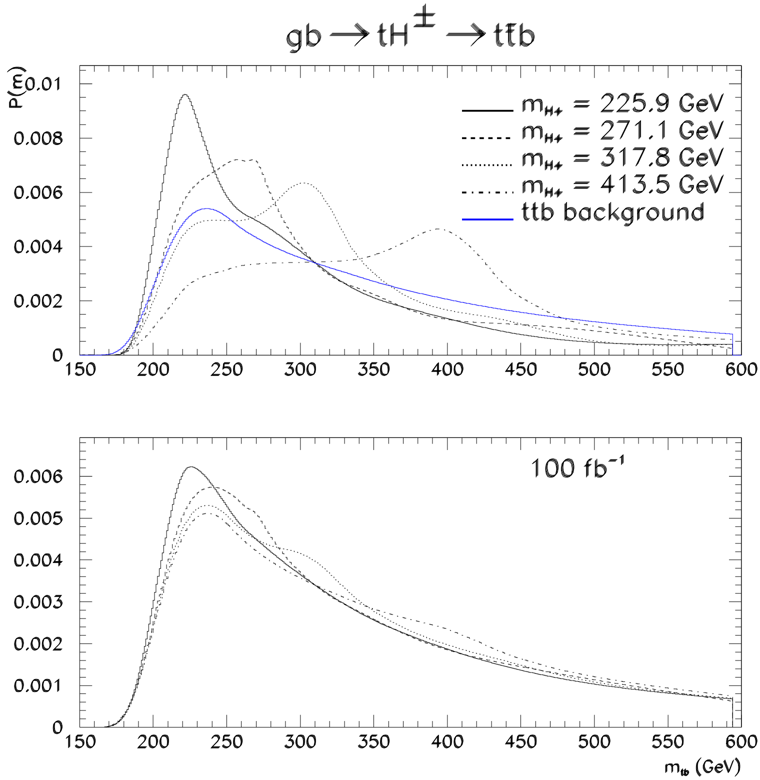

Fig. 7. The probability density functions for the signal and the background (top plot) obtained from the distributions of reconstructed tb invariant masses for the reference masses considered. The bottom plot shows the probability density functions for signal+background. In the fitting method, an exponential and a Gaussian shapes are assumed for the signal and background, respectively (see top plot).

4. Determination of $\tan\beta$

As shown in figure 1, assuming only the production processes $gb \to tH^\pm$ and $gg \to tbH^\pm$, LHC sensitivity to the discovery of the charged Higgs would be limited to the high and low $\tan\beta$ regions. The lack of sensitivity in the intermediate $\tan\beta$ region is due to the fact that the charged Higgs coupling to SM fermions is proportional to:

$$H^+ \left(m_t \cot\beta \bar{t} b_{\mathrm{L}} + m_b \tan\beta \bar{t} b_{\mathrm{R}}\right) , \tag{2}$$

the square of which goes through a minimum at $\tan\beta = \sqrt{m_t/m_b}$ [14].

The observation of a charged Higgs signal in $H^\pm \to \tau\nu$ and $H^\pm \to tb$ and the precision determination of the $m_{H^\pm}$ — as discussed above — raise the possibility of extracting $\tan\beta$ from the ratio of these two channels. The prospects of using the ratio of the rates to determine $\tan\beta$ seem even more interesting since in that case, the systematic uncertainties associated with the luminosity and the production cross section would cancel out:

$$\frac{H^\pm \to \tau\nu}{H^\pm \to tb} \simeq \frac{m_\tau^2 \tan^2\beta}{3(m_t^2 \cot^2\beta + m_b^2 \tan^2\beta)}\,. \tag{3}$$

At large $\tan\beta$, the ratio of $H^\pm \to \tau\nu$ to $H^\pm \to tb$ is unfortunately independent of $\tan\beta$ as can be seen from equation (3) [15]. Further, in the low $\tan\beta$ region, the branching fraction into $\tau\nu$ vanishes as $H^\pm \to tb$ becomes the dominant decay channel above the top-quark mass. As a result, the ratio of the $H^\pm \to \tau\nu$ to $H^\pm \to tb$ could be sensitive to $\tan\beta$ only in the intermediate $\tan\beta$ region where, as shown in figure 1, there is no discovery potential for the charged Higgs. Therefore this technique cannot be explored for the measurement of $\tan\beta$.

It is still possible to extract $\tan\beta$ by measuring the signal rate in the $\tau\nu$ channel where the backgrounds are relatively low. The main systematic error would come from the knowledge of the luminosity. The uncertainty in the rate measurement can be estimated as [16]:

$$\frac{\Delta(\sigma\times\mathrm{BR})}{\sigma\times\mathrm{BR}} = \sqrt{\frac{S+B}{S^2} + \left(\frac{\Delta\mathcal{L}}{\mathcal{L}}\right)^2}\,, \tag{4}$$

where the relative uncertainty on the luminosity measurement is taken conservatively to be 10%. The uncertainties in the rates are shown in Table IV. The uncertainty on $\tan\beta$ is computed as:

TABLE IV

The overall precisions on the rate determination in the $H^\pm \to \tau\nu$ channel for $\mathcal{L} = 30$, 100 and 300 fb^{-1}. The total number of background events is $B = 6.7$ for 30 fb^{-1} [10]. The numbers of signal events listed in the second column correspond to an integrated luminosity of 30 fb^{-1} [10].

($m_{H^\pm}$ [GeV], $\tan\beta$)	$S \equiv$ Signal events	$\Delta(\sigma\times\mathrm{BR})/(\sigma\times\mathrm{BR})$ (%)		
	30 fb^{-1}	30 fb^{-1}	100 fb^{-1}	300 fb^{-1}
200, 30	46.3	18.6	14.2	11.6
250, 40	60.3	16.9	13.3	11.2
300, 45	70.5	16.0	12.8	11.0
350, 25	18.8	28.7	19.9	14.1
400, 35	30.6	22.3	16.2	12.4
450, 60	66.9	16.3	12.9	11.1
500, 50	36.2	20.7	15.3	12.0

$$\Delta\tan\beta \simeq \Delta(\sigma\times\mathrm{BR})\left[\frac{d(\sigma\times\mathrm{BR})}{d\tan\beta}\right]^{-1} . \tag{5}$$

The cross section for $gb\to tH^\pm$ can be written as:

$$\sigma(gb\to tH^\pm)\propto m_t^2\cot^2\beta + m_b^2\tan^2\beta\,, \tag{6}$$

and the $H^\pm\to\tau\nu$ branching ratio BR_τ is:

$$\begin{aligned}\mathrm{BR}_\tau &\simeq \frac{\Gamma(H^\pm\to\tau\nu)}{\Gamma(H^\pm\to tb)+\Gamma(H^\pm\to\tau\nu)}\\ &= \frac{m_\tau^2\tan^2\beta}{3(m_t^2\cot^2\beta+m_b^2\tan^2\beta)+m_\tau^2\tan^2\beta}\,.\end{aligned} \tag{7}$$

At large $\tan\beta$, from equations (6) and (7), the rate in the $H^\pm\to\tau\nu$ channel is obtained as:

$$\sigma\times\mathrm{BR}\propto\tan^2\beta\,. \tag{8}$$

From the relations (5) and (8), we get:

$$\frac{\Delta\tan\beta}{\tan\beta}=\frac{1}{2}\frac{\Delta(\sigma\times\mathrm{BR})}{\sigma\times\mathrm{BR}}\,. \tag{9}$$

The expected uncertainties on $\tan\beta$ determination from the measurement of the rate in the $H^\pm\to\tau\nu$ channel are shown in Table V.

TABLE V

The overall precisions on $\tan\beta$ determination in the $H^\pm\to\tau\nu$ channel for $\mathcal{L}=30$, 100 and 300 fb^{-1}, and for $m_{H^\pm}=250$ GeV.

$\tan\beta$	$\Delta\tan\beta/\tan\beta$ (%)		
	30 fb^{-1}	100 fb^{-1}	300 fb^{-1}
20	15.4	10.6	7.4
25	12.2	8.7	6.5
30	10.5	7.7	6.1
35	9.1	7.0	5.7
40	8.4	6.6	5.6
45	7.7	6.6	5.5
50	7.3	6.1	5.4

5. Comparison between $H^{\pm} \to \tau\nu$ and $H^{\pm} \to tb$

The expected precisions on the charged Higgs mass determination are better in the $\tau\nu$ channel — although only a transverse mass is reconstructed — than in the tb channel, except in the low mass range where the sensitivity to the $H^{\pm} \to \tau\nu$ channel is reduced as one gets closer to the W mass threshold (see Table VI). The better expected precisions in the $\tau\nu$ channel follow from the fact that this channel offers an almost background free environment. Furthermore, for the same reasons, the $\tau\nu$ channel offers the

TABLE VI

The overall precisions on the mass determination are better in the $\tau\nu$ channel than in the tb channel. This is due to the fact that the latter suffers from large $t\bar{t}b$ and signal combinatorial backgrounds ($\mathcal{L} = 100$ fb^{-1}).

$m_{H^{\pm}}$ (GeV)	$H^{\pm} \to \tau\nu$		$H^{\pm} \to tb$	
	$< m >$	δm	$< m >$	δm
225.9	225.9	2.9	226.9	1.8
271.1	271.0	3.9	270.1	10.1
317.8	319.7	5.9	320.2	11.3
365.4	364.9	8.1	365.4	12.1
413.5	414.8	8.0	417.4	17.6
462.1	460.7	10.6	465.9	24.1
510.9	511.4	15.7		

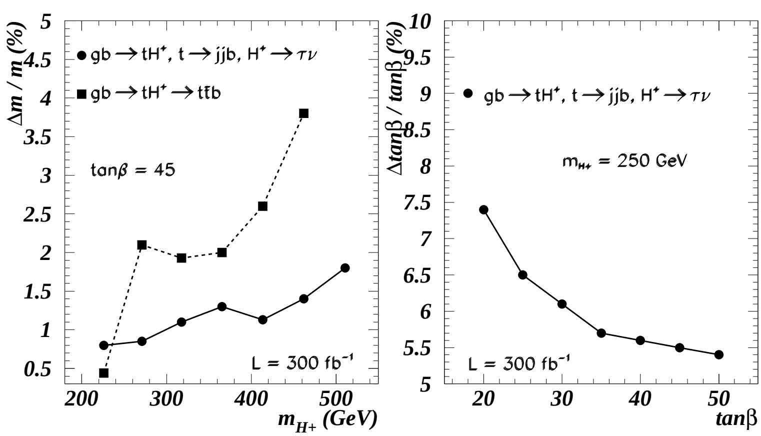

Fig. 8. The expected overall precision of the charged Higgs mass and on $\tan\beta$ measurements, as a function of the charged Higgs mass (left plot) and $\tan\beta$ (right plot) respectively. For the mass determination, the $H^{\pm} \to \tau\nu$ channel gives better precisions than $H^{\pm} \to tb$ except at low Higgs masses. In addition, $H^{\pm} \to \tau\nu$ allows for the determination of $\tan\beta$ by measuring the rate in this channel.

better opportunity of determining $\tan\beta$ from the measurement of the absolute rates. Figure 8 illustrates the expected overall precision of the charged Higgs mass and $\tan\beta$ determination for an integrated luminosity of 300 fb^{-1}.

6. Conclusions

The sensitivity of the ATLAS detector to the discovery of the charged Higgs has been studied in detail in the channels $H^\pm \to \tau\nu$, $H^\pm \to c\bar{s}$, $H^\pm \to Wh^0$ and $H^\pm \to tb$. Above the top-quark mass, the channels $H^\pm \to \tau\nu$ and $H^\pm \to tb$ provide coverage in the low and high $\tan\beta$ regions up to $\sim$600 GeV. The objective of the current analysis is to estimate the expected precisions on the charged Higgs mass and $\tan\beta$ measurements above the top-quark mass.

In the $\tau\nu$ channel, there is no resonance peak, only the transverse mass is reconstructed. A likelihood method is used to estimate the expected precisions on the mass measurements. The systematic effects include the background shape, the background rate and the energy scale. The overall relative precision in this channel ranges from 1.3% at $m_{H^\pm} = 226$ GeV to 3.1% at $m_{H^\pm} = 511$ GeV for an integrated luminosity of 100 fb^{-1}. At 300 fb^{-1}, the precision improves to 0.8% at $m_{H^\pm} = 226$ GeV and 1.8% at $m_{H^\pm} = 511$ GeV.

The tb channel offers the possibility for the reconstruction of the resonance peak above a large $t\bar{t}b$ and the signal combinatorial background. It is possible to use the likelihood method for the mass determination in this channel. Alternatively, a fit of the signal and background can be performed provided the background shape and normalization can be determined by fitting outside the signal region. Results from both methods are in agreement. The relative precision in this channel ranges from 0.8% at $m_{H^\pm} = 226$ GeV to 5.2% at $m_{H^\pm} = 462$ GeV for 100 fb^{-1}. For 300 fb^{-1}, the precision improves to 0.5% at 226 GeV and 3.5% at 462 GeV.

In either channel, the overall uncertainties are dominated by the statistical errors. The $\tau\nu$ channel offers better precisions on the Higgs mass determination than the tb channel, except at low Higgs masses where the $\tau\nu$ channel suffers from a much reduced selection efficiency or a much higher background level.

The determination of $\tan\beta$ can be achieved by measuring the rate in the $H^\pm \to \tau\nu$ channel where the background is relatively low and the discovery reach is extended to high masses compared to $H^\pm \to tb$. Assuming a 10% uncertainty on the luminosity, the relative precision of $\tan\beta$ ranges from 15.4% to 7.3% for $\tan\beta = 20$ to 50, at low luminosity. For an integrated luminosity of 300 fb^{-1}, the precision improves to: 7.4% at $\tan\beta = 20$ and to 5.4% at $\tan\beta = 50$.

The authors express gratitude to Karl Jakobs and Elżbieta Richter-Wąs for useful discussions and comments.

REFERENCES

[1] P.H. Nilles, *Phys. Rev.* **110**, 1 (1984); H. Haber, G. Kane, *Phys. Rev.* **115**, 75 (1985).

[2] ATLAS Detector and Physics Performance Technical Design Report, LHCC 99-14/15.

[3] T. Sjöstrand, High-Energy Physics Event Generation with PYTHIA 5.7 and JETSET 7.4, CERN preprints-TH.7111/93 and CERN-TH.7112/93, *Comput. Phys. Commun.* **82**, 74 (1994).

[4] E. Richter-Wąs *et al.*, ATLAS Internal Note ATL-PHYS-98-131.

[5] D. Cavalli *et al.*, ATLAS Internal Note ATL-PHYS-94-053 (1994).

[6] M. Dress, M. Guchait, D.P. Roy, *Phys. Lett.* **B471**, 39 (1999) and the references therein.

[7] K.A. Assamagan, *Acta Phys. Pol.* **B31**, 881 (2000), ATLAS Internal Note ATL-PHYS-99-025.

[8] Discussions in the charged Higgs working group, Les Houches workshop, Physics at TeV Colliders, May 21–June 01, 2001.

[9] K.A. Assamagan, *Acta Phys. Pol.* **B31**, 863 (2000), ATLAS Internal Note ATL-PHYS-99-013.

[10] K.A. Assamagan, Y. Coadou, ATLAS Internal Note ATL-PHYS-2000-031 (2000).

[11] D.P. Roy, *Phys. Lett.* **B459**, 607 (2000).

[12] R. Kinnunen, CMS Note 2000/045, `hep-ph/0002258`.

[13] M. Hohlfeld, ATLAS Internal Note ATL-PHYS-2001-004 (2001).

[14] H. Baer, M. Bisset, D. Dicus, C. Kao, X. Tata, *Phys. Rev.* **D47**, 1062 (1993).

[15] J.F. Gunion, H.E. Haber, G.L. Kane, S. Dawson, *The Higgs Hunter's Guide*, Addison-Wesley, Reading, MA 1990, Erratum: University of California, Santa Cruz, preprint SCIPP-92-58, February 1993, `hep-ph/9302272`.

[16] J.F. Gunion *et al.*, `hep-ph/9703330`.